Journal of Cleaner Production 243 (2020) 118562

Contents lists available at ScienceDirect

Journal of Cleaner Production

journal homepage: www.elsevier.com/locate/jclepro

Analysis of a clean hydrogen liquefaction plant integrated with a geothermal system

Shaimaa Seyam*, Ibrahim Dincer, Martin Agelin-Chaab

Dept. of Automotive, Mechanical and Manufacturing Engineering, Faculty of Engineering and Applied Science, Ontario Tech Univeristy, Oshawa, Canada

ARTICLE INFO

Article history:
Received 30 March 2019
Received in revised form
19 September 2019
Accepted 22 September 2019
Available online 26 September 2019

Handling editor: Kathleen Aviso

Keywords:
Cleaner production
Hydrogen liquefaction
Energy
Exergy
Efficiency
Geothermal power system

ABSTRACT

Hydrogen is attracting a lot of attention because of its high-energy content and lower weight and volume, making it a promising replacement of fossil fuels. Hydrogen liquefaction is an energy-intensive process that requires high electrical power. This paper presents a novel approach of a large-scale hydrogen liquefaction system combined with geothermal and isobutene power plant. The hydrogen liquefaction system uses a hydrogen Claude refrigeration system and a nitrogen precooling system to produce 335 ton/day of liquefied hydrogen. The mass flow rate of hydrogen in the refrigeration system and nitrogen precooling system were 14 kg/s and 52 kg/s, respectively, to produce specific energy consumption of 6.41 kWh/kg-LH_2. The overall power consumption of the liquefaction system was 107 MW. This requires constructing three geothermal and isobutene power plants to produce 130 MW of electrical power. Some parametric studies were conducted to reduce the specific energy consumption (SEC). It is found that reducing the hydrogen mass flow rate to 9 kg/s and the high pressure to 20 bar results in the reduction of the SEC to 4.7 kWh/kg-LH_2. However, increasing the steam and isobutene mass flow and high pressure in the system results in an increase in the electric power delivered to 225 MW from 130 MW.

1. Introduction

Hydrogen is a plentiful and accessible element, which has unique characteristics such as lower weight and volume and high energy content. Hydrogen is a promising clean and a high-energy carrier for storage within a set of energy storage systems (Uyar and Beşikci, 2017; Won et al., 2017). The process of hydrogen liquefaction is an energy-intensive process because of the high compression processes of refrigerants in cryogenic systems to achieve a low temperature of −253 °C. Several methods used for hydrogen production can be classified in two essential categories as a fossil fuel driven and a clean energy driven. The fossil fuel approach includes natural gas reforming, partial oxidation, and coal gasification, which produce carbon monoxide and carbon dioxide and pollute the environment. On the other hand, the clean approach includes nuclear electrolysis and thermo-chemical splitting water electrolysis, photo electrochemical, and photo-biological (Dincer and Zamfirescu, 2016).

Several studies have been conducted on large-scale hydrogen liquefaction systems. Bracha et al. (1994) presented an overview of an industrial size of hydrogen liquefaction plant that was constructed by Linde company at Ingolstadt, Germany. The daily capacity of the liquefied hydrogen is 4.4 tons using a nitrogen precooling Claude cycle. The feed of hydrogen gas was at 20 bar and 308 K, while the liquefied hydrogen product was at 1.3 bar and 21 K. The thermal efficiency of the plant is 33% concerning an ideal Carnot cycle with four stages of ortho-para conversion.

In addition, Berstad et al. (2010) investigated the use of mixed-refrigerant with the asset of pre-cooling and helium/neon cooling cycle using the system by (Quack, 2002) as a reference case. The hydrogen feed is 1 kg/s at 21 bar and 310 K, and the specific energy consumption was 6.152 kWh/kg-LH_2. This was less than the reference case by 2.9% if the liquid expander is used instead of a throttling valve to produce 86.4 ton per day of liquid hydrogen. Krasae-in et al. (2010) presented a modified large-scale liquid-hydrogen plant using mixed-refrigerant and four-hydrogen Joule-Brayton refrigeration cycles to produce 100 ton/day LH_2. The feed gaseous hydrogen is at 21 bar and 298 K. The total shaft work from all compressors is 25,190 kW to produce the overall specific energy consumption of 5.91 kWh/kg-LH_2.

* Corresponding author.
E-mail addresses: shaimaa.seyam@ontariotechu.net (S. Seyam), Ibrahim.dincer@uoit.ca (I. Dincer), Martin.Agelin-Chaab@uoit.ca (M. Agelin-Chaab).

https://doi.org/10.1016/j.jclepro.2019.118562
0959-6526/

Nomenclature

Symbols

C	Conversion coefficient
G	Gravitational acceleration, m/s^2
H	Specific enthalpy, kJ/kg
H_2	Hydrogen
K	Conversion percentage,%
LH_2	Liquefied hydrogen
n	Number of moles, kmole
N_2	nitrogen
P	Pressure, KPa
R	Gas universal constant
S	Entropy, kJ/K
s	Specific entropy, kJ/kg.K
T	Temperature, K
V	Velocity, m/s
X	Molar fraction
X	Mass fraction
$\dot{m}$	Mass flow rate
$\dot{Q}$	Heat transfer, kW
$\dot{W}$	power, kW
$\dot{E}x$	Exergy flow rate, kW

Greek symbols

μ	Chemical potential
η	Energetic efficiency
ψ	Exergetic efficiency

Abbreviations

AC	air cooling condenser
CM	compressor
CN	condenser
COP	coefficient of performance
EOS	equation of state
ET	expansion turbines or expanders
EX	expansion valve
HCR	hydrogen Claude refrigeration cycle
HPP	high pressure path
HX	heat exchanger
IT	isobutene turbine
LMTD	Logarithmic mean temperature difference
LP	liquefaction path
LPP	Low pressure path
MPP	Medium pressure path
MTA	Minimum temperature approach
MX	Mixers
NPC	Nitrogen precooling cycle
P	Pump
PEM	Proton exchange membrane
REC	reactors
S	Flash separator
SEC	specific energy consumption, kWh/kg-LH_2
SP	Splitters

Subscripts

cd	cold side
ch	chemical
cn	condenser
cv	closed volume
des	destruction
e	electrolyzer system
f	flash separators
gen	generation
geo	geothermal
ht	hot side
e	electrolyzer system
i	inlet
ith	number of components in the mixture
in	inflow
iso	isobutene system
o	outlet
out	outflow
overall	overall system
p	pump
P	products
ph	physical components
R	reactors
s	source
t	turbine
th	thermal
w	work
1,2,3, …,n	equipment number

Moreover, Baker and Shaner (1978) have performed a parametric study for a large scale of 250 ton per day liquefied hydrogen process cooled by nitrogen and semi-closed hydrogen Claude cycle. The ultimate realistic case was selected for a feed gaseous hydrogen at 1 bar and 310 K and liquefied at 9.29 bar and 20.57 K with 97% para fraction. This resulted in the overall specific energy consumption of 10.85 kWh/kg-LH_2, the overall thermal efficiency of 23.7%, and the liquefier efficiency alone was 36%.

Also, Valenti and Macchi (2008) presented a developed large hydrogen liquefier using four helium recuperative Joule-Brayton cycles. The gas hydrogen entered at 10 kg/s (860 ton/day) at 60 bar and 300 K and liquefied at 1.5 bar, 20 K and 99.8% para fraction. This developed system has a specific energy consumption of 5.29 kWh/kg-LH_2 and exergy efficiency of 48% respectively. Cardella et al. (2017) presented a novel approach for the development of the process of large scale hydrogen liquefaction. They included two processes: a combination of precooled and cryogenic refrigeration cycle (e.g., high-pressure mixed-refrigerant and high-pressure hydrogen cycles (Case A), and mixed-refrigerant and helium/neon cycles (Case B). They have found that Case A achieves a minimum specific energy consumption of 5.9 kWh/kg-LH_2 for 100 ton/day and higher exergy efficiency of 43% for feed gas hydrogen at 20 bar and 300 K.

Recent studies have been presented in this field. Ansarinasab et al. (2019) simulated a conceptual design of large-scale hydrogen liquefaction using Aspen HYSYS to produce 3.36 kg of liquefied hydrogen. The process includes a liquefaction stream and two mixed-refrigerants refrigeration cycles. The mass flow rates of both refrigeration cycles are 98 and 31.8 kg/s, respectively. The purpose of the study was to examine the exergy analysis to assess the performance of the process and the exergoeconomic to evaluate the effect of cost and economy on performance. Additionally, the exergoenvironmental analysis is used to estimate the process performance on environmental conditions. The results show that the specific energy consumption of the last stage was obtained to be 1.102 kWh/kg-LH_2. Also, the exergy efficiency of the whole process

was 55.47%. Further, the heat exchangers have the highest exergy destruction rate, the compressors and pumps produced high exergoeconomic factors due to their high cost. The pump and expanders produce high exergoenvironmental factors.

In addition, Sadaghiani et al. (2017) proposed a conceptual design of the hydrogen liquefaction process that includes a hydrogen feed stream and a mixed-refrigerants refrigeration cycle. The hydrogen stream was fed at 5400 kg/h (1.5 kg/s) at 25 °C and 21 bar. Whereas the mixed refrigerant was fed at 307,980 kg/h (85.55 kg/s). The liquefied hydrogen was produced at 1.47 kg/s. This process has a specific energy consumption of 7.646 kWh/kg-LH_2, and the coefficient of performance of the whole process is 0.0672. Also, the exergy efficiency is 32%, and the highest exergy destruction was obtained in the heat exchangers. The compressors and heat exchangers have high exergoeconomic factors.

Moreover, Ansarinasab et al. (2017) designed a hydrogen liquefaction process utilizing five refrigeration cycles to produce 1.157 kg/s. The refrigeration cycles are four single-stage refrigeration cycles using hydrogen as refrigerant, and a mixed-refrigerant refrigeration cycle. The mass flow rates are 3.33, 3.33, 2.78, and 2.22 kg/s for four hydrogen refrigeration cycles and 36.80 kg/s for a mixed-refrigerant refrigeration cycle. The specific energy consumption was not calculated in this study. However, the total power of compressors and turbines are 44241.07 kW and 3110.3 kW, respectively. Therefore, the specific energy consumption can be calculated to be 9.875 kWh/kg-LH_2. An enhanced exergy analysis was conducted, and it was found that the compressors have high exergoeconomic factors, but the heat exchangers have low exergoeconomic factors and the highest exergy destruction rate.

Furthermore, Asadnia and Mehrpooya (2017) presented a conceptual design of a hydrogen liquefaction process to produce 1.157 kg (100 ton per day) of liquefied hydrogen. The process includes precooling cycles of main mixed-refrigerant and auxiliary hydrogen refrigeration cycles, and the cryogenic cycle of six combined Joule-Brayton cascade cycle using a mixture of hydrogen and helium. The specific energy consumption was obtained to be 7.69 kWh/kg-LH_2. The coefficient of performance was 0.171. The exergy efficiency of the whole process was obtained to be 39.5%.

Hydrogen liquefaction system requires intensive electrical power to operate compressors. For example, the net power consumption can reach to 22.8 MW for 1 kg/s liquefied hydrogen (Bracha et al., 1994) and 24.2 MW for 1.033 kg/s liquefied hydrogen (Aasadnia and Mehrpooya, 2018). Therefore, alternative pathways using renewable resources are required to produce the electrical energy demand. The use of such an inexhaustible and clean source is essential for hydrogen production to lower environmental pollution. The main component becomes the water electrolysis process. Mohammadi and Mehrpooya (2018) presented a comprehensive review of the electrolyzer and their coupling to renewable sources. There are five renewable sources, including wind energy, ocean thermal conversion system, solar energy, hydroelectric energy, and geothermal energy. The main purpose of such a combination is to provide electricity and heat to split the water into hydrogen and oxygen.

Hydrogen liquefaction systems have been combined with geothermal systems in several techniques (Ohlig and Decker, 2014; Ratlamwala et al., 2012). Under realistic conditions, 7572 kW power can be produced in a combined flash binary geothermal power plant to liquefy 0.1044 kg/s of hydrogen. The energy efficiencies of the geothermal power plant and the overall system are 10.4% and 5.25%. Ratlamwala et al. (2012) have undertaken parametric studies on an integrated geothermal quadruple effect absorption system (QEAS) for hydrogen liquefaction, power and cooling productions.

In the open literature, few studies have presented a conceptual design of an integrated hydrogen liquefaction process with a renewable energy source. Therefore, the novelty of the current study is to design a complete liquefaction process starting from providing electricity and heat using renewable sources such as geothermal power plant and isobutene power plant to provide electrical energy demand for an electrolyzer and an actual hydrogen liquefaction system as reported in (Ohlig and Decker, 2014). The liquefaction process includes a closed nitrogen precooling cycle, hydrogen Claude refrigeration cycle, and a liquefaction stream. This will facilitate the production of more than 330 ton/day LH_2. The objective of this paper is to analyze the system energetically and exergetically and estimate the energy and exergy efficiencies for the system and its components. In addition, we will evaluate the energy and exergy destructions and the energy destruction ratio for all the system components as well as to conduct parametric studies to reduce the specific energy consumption and improve the thermal efficiency of the liquefaction system.

2. System description

The state-of-the-art of a liquefaction process consists of three main stages: precooling, cryogenic, and liquefying stream. The first two stages are combined with compressors, expanders, condensers, and heat exchangers. The electric power is required for operating the two first stages and the electrolyzer. This power can be provided by two geothermal and isobutene power plants, as simplified in Fig. 1.

The system consists of renewable energy supply and large-scale hydrogen liquefaction subsystems, as shown in Fig. 2. The renewable energy supply subsystem is a combination of a single-flash geothermal system and an isobutene Rankine system to provide electricity from non-fossil fuels products, which can be performed by using heat from underground, as shown in Fig. 1. The geothermal system is composed of a production well to produce saturated liquid steam at 250 °C through a flash chamber at a pressure of 1000 kPa. This chamber is connected to a flash separator to split the saturated vapour to a turbine at 1000 kPa and a saturated liquid to the heat exchanger HX1 which is cooled down to 82.57 °C by heating the isobutene in the isobutene power cycle. The exiting steam from the turbine at 80 kPa enters a condenser CN1 and leaves in the liquid phase at 93.18 °C to be mixed at the exit of expansion valve EX1 to enter the reinfection well at 93.13 °C and 80 kPa. The isobutene power cycle consists of the turbine (IT), a heat exchanger (HX1), pump (P1), and air cooling condenser (AC). The steam and isobutene mass flow rates are 500 kg/s and 400 kg/s, respectively.

The net power produced by these two power plants is used for the water electrolyzer and the hydrogen liquefaction system. The water's mass flow rate of 32.09 kg/s enters the electrolyzer to produce 3.566 kg/s of hydrogen and 28.52 kg/s of oxygen. The thermodynamic analysis was applied to the isobutene and geothermal power plants and electrolyzer using the Engineering Equation Solver (EES) software because it contains the necessary functions along with built-in thermodynamic tables and the properties of isobutene and steam/water.

The hydrogen liquefaction subsystem consists of two cycles and a chain, as shown in Fig. 2. The first cycle is the hydrogen Claude refrigeration cycle (HCR), which is the main refrigeration system to liquefy the hydrogen of 3.5155 kg/s (340 ton/day) through the chain of liquefaction. The other cycle is the nitrogen precooling cycle (NPC). The HCR consists of two compressors (CM1, and CM2) to raise the hydrogen pressure from 200 kPa to 2500 kPa, two condensers (CN2 and CN3) to cool the heated hydrogen to almost room temperature, eight expansion valves (EXs), nine plated-fin heat exchangers (HXs) and eight of them are filled with the catalyst (the iron (III) hydroxide ($Fe(OH)_3$)) for the liquefied hydrogen stream,

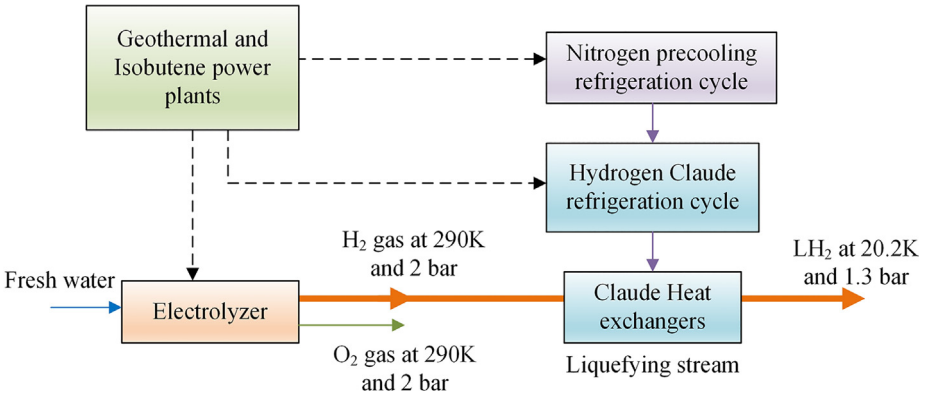

Fig. 1. Layout of the whole hydrogen liquefaction process.

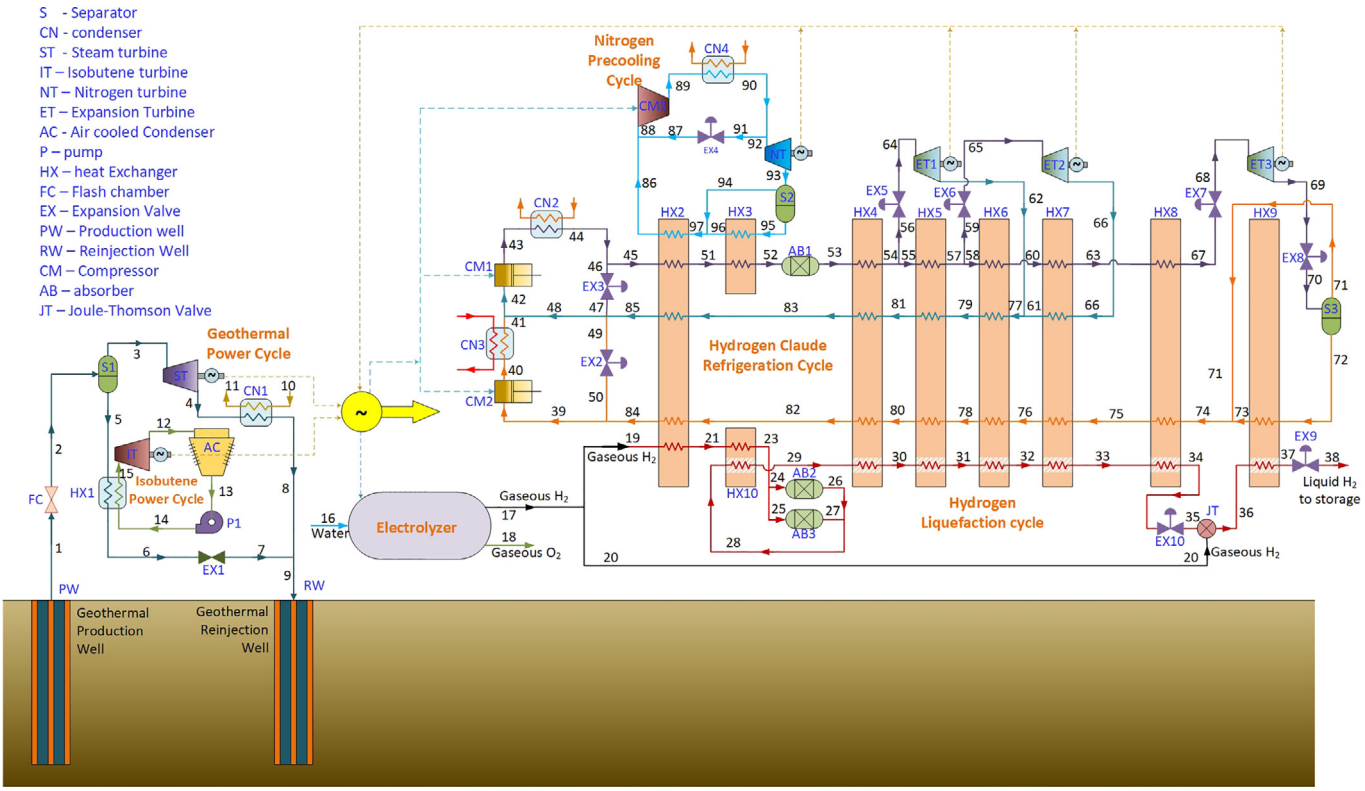

Fig. 2. Schematic diagram of an integrated geothermal power plant with an electrolyzer and a hydrogen liquefaction system.

three expanders (ETs), and a flash separator (S3). There are four main paths: high-pressure path (HPP) of 2500 kPa, medium-pressure path (MPP) of 1000 kPa, low-pressure path (LPP) of 200 kPa, and liquefaction path (LP). The cold paths are HPP and LP, while the hot paths are MPP and LPP. The HPP exits from HX4 and splits into two: one enters expansion valve EX5 and expander ET1 and exits at 1000 kPa to combine with the MPP and enters HX5. The other enters the next heat exchanger HX5. Similarly, the HPP exits from HX5 and splits into two parts: one enters expansion valve EX6 and expander ET2 and exits at 1000 kPa to enter HX7. The other enters the following heat exchanger HX6. The HPP exit from the heat exchanger HX8 and enters the expansion valve EX7, expander ET3, and expansion valve EX8 to lower the pressure to 200 kPa and enters the flash separator S3.

The second cycle is the nitrogen precooling cycle (NPC), which consists of three compressors, three condensers, a turbine, a flash separator, two heat exchangers HX2 and HX3, and an expansion valve EX4, as shown in Fig. 2. The nitrogen gas is compressed from 100 kP to 20000 kPa and is cooled down in the condensers to a range of 230 K–290 K. Then, it is expanded in the turbine to 100 kPa where the flash separator splits the vapour and liquid phase at a temperature of 77.3655 °C. The liquid nitrogen cools the hot hydrogen in HX3 and is heated to more than 80 K and is mixed with saturated vapour nitrogen of a temperature of about 78C, then the cold gas nitrogen cools the hot hydrogen to reach 290 K. Fig. 3 shows the T-s diagrams for nitrogen, gaseous hydrogen and liquefied hydrogen cycles.

The process flow of the hydrogen liquefaction system was applied using Aspen Plus, as shown in Fig. 4. Pure nitrogen, hydrogen, and para-hydrogen properties are calculated with the

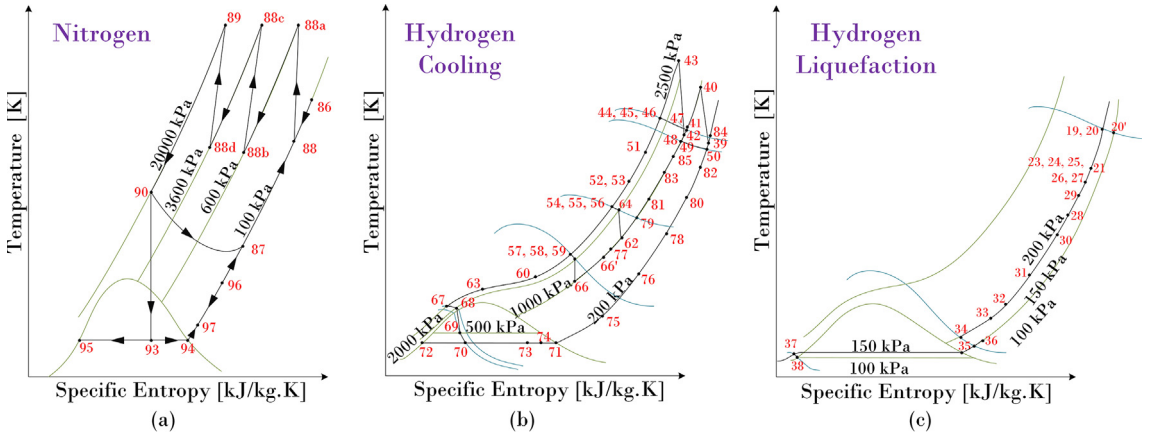

Fig. 3. T-s diagrams for nitrogen precooling cycles (a), hydrogen Claude refrigeration system (b), and hydrogen liquefaction (c).

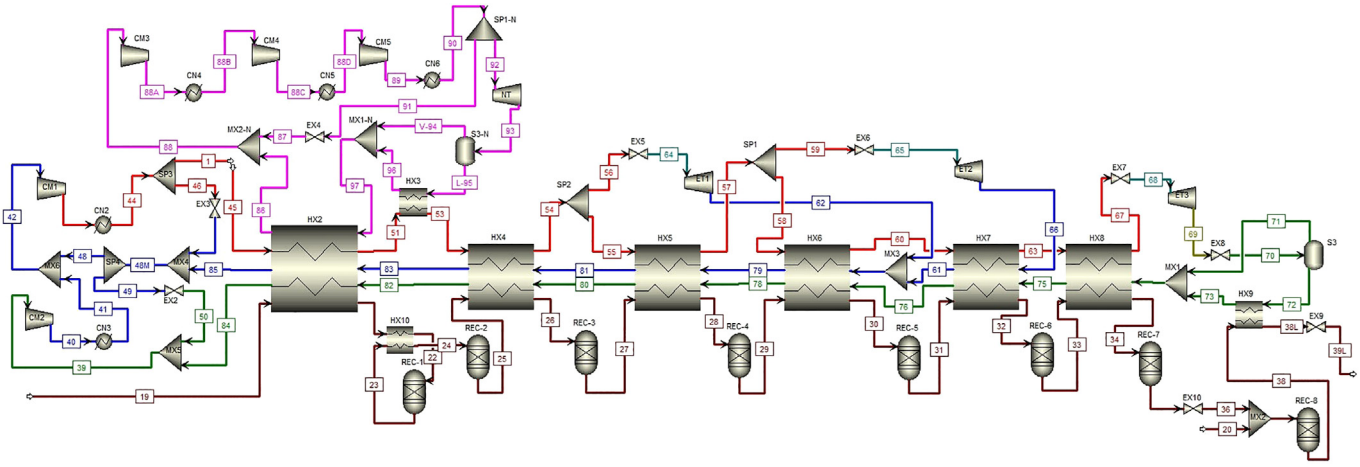

Fig. 4. Aspen PLUS flowsheet for the hydrogen liquefaction system.

equation of state (EOS) implemented in the Peng-Robinson model, which has been recommended and used for refrigeration and liquefaction processes (Leachman et al., 2009; Noh et al., 2017; Peng and Robinson, 1976). The nitrogen and hydrogen Claude refrigeration cycles are used nitrogen and gaseous hydrogen, which are simulated with the gaseous-hydrogen fluid properties [46], while the liquefied hydrogen is implemented as a combination of gaseous and para-hydrogen using the Peng-Robinson model. The conversion of normal hydrogen into para-hydrogen is carried out through a catalyst bed in the heat exchangers, as shown in Fig. 2. However, this option is not implemented in the Aspen Plus, so a series of eight conversion reactors (REC-1 to REC-8) are added after each heat exchanger. These reactors are exothermic, isothermal and isobaric reactors.

2.1. System analysis

Thermodynamic analysis was performed on the system in order to evaluate the system performance. Some assumptions are considered as follows:

- No pressure drops in pipes and heat exchangers.
- No heat losses in pipes, turbines, compressors, condensers, heat exchangers, and flash separators.
- Turbines and compressors have thermal isentropic efficiencies within 80% and optimal mechanical efficiencies.
- The kinetic and potential energies are neglected since the changes in velocities and elevation across the system are small compared to flow energy, work, and heat.
- All processes are performed under steady state conditions.

2.1.1. Balance equations

Three balance equations are studies for each components: mass, energy, and exergy balance equations. The mass balance equation for a steady state flow process is expressed in a general form as

$$\sum \dot{m}_{in} = \sum \dot{m}_{out} \tag{1}$$

The energy balance equation for steady flow process can be generalized to be as the following equation:

$$\dot{Q}_{cv} - \dot{W}_{cv} + \sum \dot{m}_i \left(h_i + \frac{1}{2} V_i^2 + g z_i \right) - \sum \dot{m}_o \left(h_o + \frac{1}{2} V_o^2 + g z_o \right) = 0 \tag{2}$$

where $\dot{Q}_{cv}$ and $\dot{W}_{cv}$ represents the heat transfer and the work crossing the boundaries of system of. The steady energy flow is expressed as $(h + 0.5V^2 + gz)$, which represents kinetic energy,

and the specific enthalpy, V is the stream velocity of the working fluid, g is the gravitational acceleration, and z is the elevation from a reference point. Also, the exergy balance equation for a steady flow process can be expressed as

$$\sum \dot{m}_{in} ex_{in} = \sum \dot{E}x_{th} + \sum \dot{E}x_{w} + \sum \dot{m}_{out} ex_{out} + \dot{E}x_{des} \quad (3)$$

where $\dot{E}x_{th}$ denotes the thermal exergy with the heat energy exchange across the system volume and is expressed as $\dot{E}x_{th} = (1 - T_o/T_s)\dot{Q}$. $\dot{E}x_w$ denotes the rate of exergy transfer by the boundary or work applied on or done by the system $\dot{E}x_w = \dot{W}$. The total specific exergy of each stream is comprised of physical $ex_{ph,i}$ and chemical exergy $ex_{ch,i}$ and can be described as the following:

$$ex_i = ex_{ph,i} + ex_{ch,i} \quad (4)$$

$$ex_{ph,i} = (h_i - h_o) - T_o(s_i - s_o) \text{ and } ex_{ch,i} = \sum n_i(\mu_i^o - \mu_i^\infty) \quad (5)$$

where s is the specific entropy, subscript o stands for dead state, T_o is the ambient temperature, μ_i^o is the chemical potential of ith component in thermomechanical equilibrium, and $\mu_i^\infty$is chemical potential of ith component in chemical equilibrium. In addition, the specific exergy $\dot{E}x_{ch} = \dot{m}\, ex_{mix}^{ch}$ of the gas mixture can be expressed as equation (6), where x_i is defined as the molar fraction of a gas i in the gas mixture.

$$ex_{mix}^{ch} = \left[\sum_{i=1}^{n} x_i ex^{c,i} + RT_o \sum_{i=1}^{n} x_i ln x_i\right] \quad (6)$$

The proposed systems consist of turbines, compressors, pump, flash separators, heat exchangers, condensers, and expansion valves. Therefore, the mass, energy, exergy balance equations are expressed in a general form and listed in Table 1.

2.1.2. Electrolyzer

Water electrolysis is the most developed method for hydrogen production by using clean resources to replace fossil fuels. In this paper, a proton exchange membrane (PEM) electrolysis is used for hydrogen production via electrochemical conversion of water to hydrogen and oxygen. The PEM electrolyzer consists of two electrodes and an electrolyte (Carmo et al., 2013; Dincer and Acar, 2014). Water is fed to the anode at 290 K and 2 bar, where it is split into oxygen and H^+. Then, the produced proton is transferred through the membrane to the cathode, where it receives electron and forms hydrogen. The reaction regarding the hydrogen production in the PEM electrolyzer can be written as

$$\text{Overall reaction: } 2H_2O + \Delta H \rightarrow 2H_2 + O_2 \quad (7)$$

$$\text{Anodic reaction (oxidation)}: \ 2H_2O \rightarrow O_2 + 4H^+ + 4e^- \quad (8)$$

$$\text{Cathodic reaction (reduction)}: \ 2H^+ + 2e^- \rightarrow H_2 \quad (9)$$

When the second-law of thermodynamics is applied to the electrolysis process, the total obtained work (exergy) needed for the electrolyzer can be obtained as

$$\dot{W}_e = \Delta G = \Delta H - T\Delta S \quad (10)$$

where ΔG is Gibb's free energy, which is the electrical energy demand to operate the electrolyzer, ΔH is the theoretical energy required for water electrolysis without any loss, and $T\Delta S$ represents the thermal energy requirement. In addition, the mass, energy and exergy balance equations of PEM electrolyzer are obtained using the EES software as shown in Table 1.

2.1.3. Power requirement

The main purpose is to provide electricity from non-fossil fuels products, which can be performed by using heat from underground. This can be achieved using geothermal power plant combined with isobutene power plant to provide electrical demand of both electrolyzer and hydrogen liquefaction, as shown in Fig. 1. The net power of binary flash geothermal and isobutene power plants are written as

$$\dot{W}_{net} = \dot{W}_{t,\,geo} + \dot{W}_{t,\,iso} - \dot{W}_{p,iso} \quad (11)$$

This net power should exceed the required power of hydrogen liquefaction process, which is a combination of compressors and turbines of the NPC and HCR cycles. The excess electricity can be added to the electric grid for community services, given below:.

$$\dot{W}_{net} = \sum_{N_2} \dot{W}_t - \dot{W}_c + \sum_{H_2} \dot{W}_t - \dot{W}_c + \dot{W}_{excess} \quad (12)$$

2.1.4. Ortho-para hydrogen conversion reactors

The gaseous hydrogen is composed of two nuclear spins of atoms called as ortho-hydrogen and para-hydrogen and are function of temperature only. The nuclear spins of ortho-hydrogen and para-hydrogen are parallel and antiparallel, respectively. At the

Table 1
Mass, energy, exergy balance equations for basic components in the integrated system.

Components	Mass balance	Energy balance	Exergy balance
Compressors	$\dot{m}_{in,c} = \dot{m}_{out,c}$	$\dot{W}_c = \dot{m}_c(h_{out,c} - h_{in,c})/\eta_c$	$\dot{m}_{in,c}ex_{in,c} + \dot{W}_c = \dot{m}_{out,c}ex_{out,c} + \dot{E}x_{des,c}$
Turbines	$\dot{m}_{in,t} = \dot{m}_{out,t}$	$\dot{W}_t = \eta_t\dot{m}_t(h_{in,t} - h_{out,t})$	$\dot{m}_{in,t}ex_{in,t} = \dot{W}_t + \dot{m}_{out,t}ex_{out,t} + \dot{E}x_{des,t}$
Pumps	$\dot{m}_{in,p} = \dot{m}_{out,p}$	$\dot{W}_p = \dot{m}_p(h_{out,p} - h_{in,p})/\eta_p$	$\dot{m}_{in,p}ex_{in,p} + \dot{W}_p = \dot{m}_{out,p}ex_{out,p} + \dot{E}x_{des,p}$
Condensers	$\dot{m}_{in,cn} = \dot{m}_{out,cn}$	$\dot{Q}_{cn} = \dot{m}_{cn}(h_{out,cn} - h_{in,cn})$	$\dot{m}_{in,cn}ex_{in,cn} = (1 - T_o/T_s)\dot{Q}_{cn} + \dot{m}_{out,cn}ex_{out,cn} + \dot{E}x_{des,cn}$
Heat Exchangers	$\sum_i \dot{m}_{in,cd} = \sum_i \dot{m}_{out,cd}$	$\dot{Q}_{ht} = \sum_i \dot{m}_{ht}(h_{out,ht} - h_{in,ht})$	$\sum_i \dot{m}_{ht}ex_{in,ht} + \sum_i \dot{m}_{cd}ex_{in,cd} = \sum_i \dot{m}_{ht}ex_{out,ht} + \sum_i \dot{m}_{cd}ex_{out,cd} + \dot{E}x_{des,hx}$
	$\sum_i \dot{m}_{in,ht} = \sum_i \dot{m}_{out,ht}$	$\dot{Q}_{cd} = \sum_i \dot{m}_{cd}(h_{in,cd} - h_{out,cd})\dot{Q}_{cd} = \dot{Q}_{ht}$	
Expansion valves	$\dot{m}_{in,ex} = \dot{m}_{out,ex}$	$h_{in,ex} = h_{out,ex}$	$\dot{m}_{in,ex}ex_{in,ex} = \dot{m}_{out,ex}ex_{out,ex} + \dot{E}x_{des,ex}$
Flash separators	$\dot{m}_{in,f} = \sum \dot{m}_{out,f}$	$\dot{m}_{in,f}h_{in,f} = \dot{m}_{out,f,v}h_{out,f,v} + \dot{m}_{out,f,l}h_{out,f,l}$	$\dot{m}_{in,f}ex_{in,f} = \dot{m}_{out,f,v}ex_{out,f,v} + \dot{m}_{out,f,l}ex_{out,f,l} + \dot{E}x_{des,f}$
Reactors	$\sum_R \dot{m}_{in,R} = \sum_P \dot{m}_{out,P}$	$\sum_R \dot{m}_{in,R}h_{in,R} = \dot{Q}_{out,r} + \sum_P \dot{m}_{out,P}h_{out,P}$	$\sum_R \dot{m}_{in,R}ex_{in,R} = (To/Ts, r - 1)\dot{Q}_{out,r} + \sum_P \dot{m}_{out,P}ex_{out,P} + \dot{E}x_{des,r}$
Electrolyzer	$\dot{m}_w = \dot{m}_{O_2} + \dot{m}_{H_2}$	$\dot{W}_e + \dot{m}_{w,R}h_{w,R} = \dot{m}_{O_2}h_{O_2} + \dot{m}_{H_2}h_{H_2}$	$\dot{W}_e + \dot{m}_{w,R}ex_{w,R} = \dot{m}_{O_2}ex_{O_2} + \dot{m}_{H_2}ex_{H_2} + \dot{E}x_{des,e}$

ambient temperature, the gaseous hydrogen contains 75% ortho-hydrogen and 25% para-hydrogen (McCarty et al., 1981). By decreasing the temperature to 20 K, the amount of para-hydrogen is increased to 99.8% while the amount of ortho-hydrogen is decreased to 0.2%. This conversion is important because the existence of para-hydrogen in the liquid state stabilizes the liquid phase for a long period, while the liquefactions of gaseous hydrogen at such low temperature will evaporate within 24 h (Wagner, 2014). The ortho-para hydrogen chemical conversion can be given as

$$(ortho-H_2) \rightleftarrows (para-H_2) + Heat \tag{13}$$

Here, the properties of ortho-hydrogen are not implemented in Aspen Plus. Therefore, the conversion of normal hydrogen to para-hydrogen is considered since normal hydrogen contains ortho and para-hydrogen, and the main reason for conversion reactors is to convert certain amount of normal hydrogen into para-hydrogen. Therefore, the chemical conversion can be written as:

$$X_n(normal-H_2) \rightleftarrows (1-X_p)(normal-H_2) + X_p(para-H_2) + Heat \tag{14}$$

where X_n and X_p is the mass fraction of normal and para-hydrogen, respectively. That means the total mass fraction of para-hydrogen is estimated as $Y_p = 0.25 + 0.75X_p$ while the total mass fraction of ortho-hydrogen is calculated as $Y_o = 0.75 - 0.75X_p$.

The original design of the liquefaction system is illustrated in Fig. 2, where the heat exchangers (HX4 to H10) have a catalyst for ortho-para hydrogen conversion (lower hatched box for liquefaction stream). Aspen Plus was selected for simulation the entire process. However, it cannot simulate the heat exchanger with a catalyst. Therefore, eight conversion reactors are used to replace the catalyst inside the heat exchanger for hydrogen liquefaction stream, and they are placed at the heat exchanger downstream of the liquefying path. The conversion stages are considered to be patch-continuous after each heat exchanger. The conversion percentage (K) depends on hydrogen exit temperature from the heat exchanger as (Asadnia and Mehrpooya, 2017):

$$K = C_0 + C_1T + C_2T^2 \tag{15}$$

where K is conversion percentage, and C_0, C_1, and C_2 are conversion coefficients, and T is hydrogen temperature in Kelvin. The conversion coefficients are adjusted to match para-hydrogen percentage of the reactor at certain temperature T and must equal the experimental data (McCarty et al., 1981).

2.2. System performance evaluation

The system performance can be evaluated using four parameters: overall energy efficiency, thermal energy efficiency, exergy efficiency, and specific energy consumption. The energy and exergy efficiencies of each subsystem are also estimated. The energy efficiency or the coefficient of performance (COP) is defined as the ratio of useful output energy to the consumed or required energy to operate a system, while the exergy efficiency is defined as the ratio of useful exergy to the required exergy, which measures the extent of the system performance with respect to ideal cycle. The high exergy efficiency shows that it approaches ideality. The overall energy and exergy of the hydrogen liquefaction system can be expressed as equations (16) and (17). The figure of merit (FOM) is also defined as the ratio of minimum power to the actual net power consumption of the whole process. By this definition, the FOM is expressed exactly as the exergy efficiency as

$$\eta_{overall} = \frac{\dot{m}_{LH_2}(h_{19} - h_{LH_2})}{\sum \dot{W}_c - \sum \dot{W}_t} \tag{16}$$

$$\psi_{overall} = \frac{\dot{m}_{LH_2}(ex_{19} - ex_{LH_2})}{\sum \dot{W}_c - \sum \dot{W}_t} = FOM \tag{17}$$

where $\dot{m}_{LH_2}$ is the mass of liquefied hydrogen, h_{19} and h_{LH_2} are the specific enthalpies of the feed at state point 19 and liquefied hydrogen, and $\dot{W}_c$ and $\dot{W}_t$ are the work done by a compressor and the output power of a turbine, respectively. The specific energy consumption (SEC) is defined as the ratio of the net power required to liquefy the hydrogen with respect to the amount of liquefied hydrogen as

$$SEC = \frac{\sum \dot{W}_c - \sum \dot{W}_t}{\dot{m}_{LH_2} \times 3600} \tag{18}$$

The minimum theoretical specific liquefaction power (SEC_{min}) is calculated as the difference in exergy rate between the feed and product divided by the mass flow rate of the liquefied hydrogen as defined in equation (19). Therefore, the SEC_{min} equals to 4.06 kWh/kg_{LH_2}.

$$SEC_{min} = \frac{\dot{E}x_{feed} - \dot{E}x_{product}}{\dot{m}_{LH_2} \times 3600} \tag{19}$$

Thus, the exergy efficiency also can be defined as the ratio of ideal SEC to the actual SEC and can be written as $\psi_{overall} = \frac{SEC_{min}}{SEC}$. The overall energetic and exergetic COP of nitrogen precooling cycle and hydrogen Claude refrigeration cycles can be estimated as

$$COP_{en,N_2} = \frac{\dot{Q}_{HX2} + \dot{Q}_{HX3}}{\sum \dot{W}_c - \dot{W}_t} \tag{20}$$

$$COP_{ex,N_2} = \frac{\sum_{i=2}^{3}(T_o/T_{s,i} - 1)\dot{Q}_{HXi}}{\sum \dot{W}_c - \dot{W}_t} \tag{21}$$

$$COP_{en,H_2} = \frac{\sum_{i=2}^{9}\dot{Q}_{HXi}}{\sum \dot{W}_c - \sum \dot{W}_t} \tag{22}$$

$$COP_{ex,H_2} = \frac{\sum_{i=2}^{9}(T_o/T_{s,i} - 1)\dot{Q}_{HXi}}{\sum \dot{W}_c - \sum \dot{W}_t} \tag{23}$$

where Q_{HXi} is the heat transfer to the cold streams which is equal to the heat transfer from the hot stream of the heat exchangers. The energy and exergy efficiency of the geothermal power subsystem are given as

$$\eta_{geo} = \frac{\dot{W}_t + \dot{Q}_{HX1} + \dot{Q}_{cn}}{\dot{E}_1 - \dot{E}_9} \tag{24}$$

$$\psi_{geo} = \frac{\dot{W}_t + (1 - T_o/T_s)\dot{Q}_{HX1} + (1 - T_o/T_s)\dot{Q}_{cn}}{\dot{E}x_1 - \dot{E}x_9} \tag{25}$$

where, $\dot{E}_1$ and $\dot{E}x_1$ are the energy and exergy rate of geothermal production well, and $\dot{E}_9$ and $\dot{E}x_9$ are the energy and exergy rate of geothermal reinjection well. The energy and exergy efficiencies of the isobutene power subsystem are given as:

Table 2
Thermodynamic settings and design assumptions for the integrated system.

Parameter	Remarks
Ambient condition	298 K and 101.3 kPa
Hydrogen feed	290 K and 200 kPa
LH_2 product	20 K and 130 kPa
LH_2 mass flow rate	3.5155 kg/s (335 ton/day)
Minimum temperature approach for heat exchangers	1–2 °C (arbitrary selected for high effectiveness)
Equation of State	Peng-Robinson
Inlet nitrogen conditions State 88	267.093 K, 100 kPa, 52 kg/s
Inlet hydrogen condition state 39	276.864 K, 200 kPa, 11 kg/s
Inlet hydrogen condition state 44	298 K, 2500 kPa, 14 kg/s
Production well condition State (1)	250 °C, 3974 kPa, 500 kg/s
Isobutene mass flow rate	400 kg/s
Adiabatic efficiency:	
compressors	78–85% (worst case)
turbines	80–90% (state-of-the-art turbomachinery)
pumps	60% (worst case)
Inlet water condition to Electrolyzer	17 °C, 200 kPa, 32.09 kg/s
Pressure drop in piping, connectors, mixers, splitters, heat exchangers, condensers, etc.	0 kPa (ideal case for this study)

$$\eta_{iso} = \frac{\dot{W}_t}{\dot{W}_p + \dot{Q}_{HX1}} \tag{26}$$

$$\psi_{iso} = \frac{\dot{W}_t}{\dot{W}_p + \left(1 - \frac{T_o}{T_s}\right)\dot{Q}_{HX1}} \tag{27}$$

The energy and exergy efficiencies of the electrolyzer can be written as:

$$\eta_e = \frac{\dot{m}_{H_2} h_{H_2}}{\dot{W}_e + \dot{m}_w h_w} \tag{28}$$

$$\psi_e = \frac{\dot{m}_{H_2} ex_{H_2}}{\dot{W}_e + \dot{m}_{w,R} ex_{w,R}} \tag{29}$$

Table 3
Process stream data for hydrogen liquefaction subsystem.

State	$\dot{m}$ [kg/s]	T [K]	P [kPa]	h [kJ/kg]	s [kJ/kg.K]	ex [kJ/kg]
19	3.5155	290	200	−115.74	−3.20	838.38
20	0.0001	290	150	−115.862	−2.02	484.32
21	3.5155	100	200	−2765.35	−18.00	2601.99
22	3.5155	89.49	200	−2910.53	−19.54	2914.16
23	3.5155	70	200	−3287.43	−23.36	3784.41
24	3.5155	80	200	−3142.26	−21.42	3351.58
25	3.5155	80	200	−3118.16	−20.90	3326.05
26	3.5155	68	200	−3290.58	−23.23	3849.89
27	3.5155	68	200	−3316.53	−23.78	3881.03
28	3.5155	56	200	−3491.68	−26.60	4550.92
29	3.5155	56	200	−3592.30	−30.11	4688.87
30	3.5155	44	200	−3775.42	−25.10	3010.33
31	3.5155	44	200	−3815.02	−25.64	2626.32
32	3.5155	30	200	−4035.61	−20.45	2060.35
33	3.5155	30	200	−4052.95	−19.86	5694.76
34	3.5155	22	200	−4640.02	−17.89	6081.61
35	3.5155	22	200	−4638.63	−16.35	12976.30
36	3.5155	21.60	150	−4638.63	−16.33	13302.10
37	3.5156	21.60	150	−4638.51	−16.35	13834.20
38	3.5156	20.5	150	−4668.80	−15.89	13833.90
38L	3.5156	20.2	130	−4678.62	−15.859	15467.10

3. Results and discussion

The thermodynamic analysis of three subsystems are evaluated using the EES and Aspen plus software. Also, the parametric studies have been undertaken for certain parameters to increase system efficiency and decrease the specific energy consumption of hydrogen liquefaction. The results and discussions are presented in the following subsections.

3.1. Thermodynamic analysis results

The primary assumptions for the integrated large-scale liquefaction system are listed in Table 2. The thermodynamic properties of each state of the integrated system are estimated using the EES and Aspen plus software. The thermodynamic properties of the liquefied hydrogen from state 19 to state 39L are listed in Table 3, while the specific enthalpies, entropies, and exergy rates for the hydrogen Claude refrigeration and nitrogen precooling cycles are tabulated in Tables 4 and 5. The energy and exergy rates for the components of hydrogen liquefaction system are recorded in

Table 4
Process stream data for hydrogen Claude refrigeration subsystem.

State	$\dot{m}$ [kg/s]	T [K]	P [kPa]	h [kJ/kg]	s [kJ/kg.K]	ex [kJ/kg]
39	11	276.86	200	−302.71	−3.86	848.12
40	11	479.38	1000	2625.06	−2.58	3395.5
41	11	295	1000	−42.28	−9.61	2820.86
42	14	295.35	1000	−37.21	−9.59	2820.81
43	14	406.29	2500	1570.91	−8.77	4186.24
44	14	298	2500	4.99	−13.25	3956.31
45	11	298	2500	4.99	−13.25	3956.31
46	3	298	2500	4.99	−13.25	3956.31
47	3	298.30	1000	4.99	−9.45	2820.62
48	3	296.65	1000	−18.64	−9.53	2820.67
48M	6	296.65	1000	−18.64	−9.53	2820.67
49	3	296.65	1000	−18.64	−9.53	2820.67
50	3	296.81	200	−18.64	−2.87	836.80
51	11	85	2500	−3043.18	−31.30	6287.75
53	11	80	2500	−3120.93	−32.24	6491.10
54	11	76	2500	−3184.38	−33.05	6670.26
55	10	76	2500	−3184.38	−33.05	6670.26
56	1	76	2500	−3184.38	−33.05	6670.26
57	10	73	2500	−3232.89	−33.71	6815.92
58	8	73	2500	−3232.89	−33.71	6815.92
59	2	73	2500	−3232.89	−33.71	6815.92
60	8	70	2500	−3282.38	−34.40	6972.87
61	2	63	1000	−3320.71	−31.51	6074.23
62	1	62.57	1000	−3327.29	−31.62	6098.89
63	8	60	2500	−3458.56	−37.12	7607.68
64	1	74.81	2000	−3184.38	−32.20	6415.33
65	2	71.73	2000	−3232.89	−32.86	6564.25
66	2	59.88	1000	−3368.22	−32.29	6257.31
67	8	50	2500	−3681.55	−41.21	8604.52
68	8	49.1	2300	−3681.55	−40.99	8538.20
69	8	31.69	300	−4545.04	−61.27	13722.40
70	8	30.40	200	−4545.04	−61.22	13706
71	0.34	30.40	200	−3745.14	−34.90	6660.49
72	7.66	30.40	200	−4580.54	−62.38	14018.60
73	7.66	30.40	200	−4576.03	−62.24	13978.90
74	8	30.40	200	−4540.72	−61.07	13667.90
75	8	30.40	200	−4059.75	−45.25	9431.57
76	8	30.40	200	−3798.51	−36.66	7130.64
77	3	62.86	1000	−3322.90	−31.55	6082.42
78	8	33.56	200	−3697.48	−33.41	6263.42
79	3	68	1000	−3245.75	−30.37	5807.75
80	8	41.85	200	−3576.53	−30.19	5423.46
81	3	71	1000	−3201.33	−29.73	5661.59
82	8	51.76	200	−3435.53	−27.16	4662.65
83	3	75	1000	−3142.63	−28.92	5480.48
84	8	269.36	200	−409.24	−4.25	857.89
85	3	295	1000	−42.28	−9.61	2820.86

Table 5
Process stream data for nitrogen precooling subsystem.

State	$\dot{m}$ [kg/s]	T [K]	P [kPa]	h [kJ/kg]	s [kJ/kg.K]	ex [kJ/kg]
86	42	290	100	−8.76	−0.03	0.08
87	10	171.02	100	−132.84	−0.58	39.10
88	52	267.09	100	−32.62	−0.11	0.65
88A	52	494.78	600	205.16	−6.42E-05	205.22
88B	52	290	600	−10.19	−0.56	157.32
88C	52	536.89	3600	248.91	−0.45	383.10
88D	52	285	3600	−23.84	−1.14	315.14
89	52	515.41	20000	222.88	−1.03	528.92
90	52	230	20000	−132.84	−2.05	479.10
91	10	230	20000	−132.84	−2.05	479.10
92	42	230	20000	−132.84	−2.05	479.10
93	42	77.37	100	−251.34	−1.67	246.43
V-94	37.87	77.37	100	−231.70	−1.42	190.37
L-95	4.13	77.37	100	−431.33	−4.00	760.08
96	4.13	84.16	100	−224.39	−1.32	170.69
97	42	78.03	100	−230.98	−1.41	188.33

Table 6, which includes the work added to the system or done by a system, heat rejected or added, and the heat duty of heat exchangers. Also Table 6 contains the exergy destruction rate, thermal efficiency and exergy efficiency for each component in the system. In addition, Table 7 displays the minimum temperature approach (MTA), the logarithmic meant temperature difference (LMTD), the number of paths, and the heat duty for each heat exchanger in the liquefaction process. The MTA ranges from 1.00 to 2.48 °C, and the LMTD ranges from 1.57 to 18.14 °C. The difference in MTA values is due to the temperature of hot and cold paths and the pinch temperature of heat exchangers (1–3 °C) similar to the MTA values of (Asadnia and Mehrpooya, 2017; Berstad et al., 2010; Sadaghiani and Mehrpooya, 2017).

The amount of para-hydrogen depends on the temperature of the reactor, and the reactors are isothermal, isobaric and exothermic because the reactors operates under constant pressure and temperature for each stage and releases heat due to conversion from normal to para-hydrogen based on equation (8). Table 8 displays the reactor temperature and the mass fraction of normal hydrogen $(1-X_p)$ and para-hydrogen (X_p) as well as the mass fraction of total para-hydrogen (Y_p). Also, Table 7 presents the conversion coefficients from C_0, C_1, and C_2 and the conversion percentage K for each reactor at a specific hydrogen temperature. The rejected heat from the reactors, the exergy destruction rate, and energy and exergy efficiencies are listed in Table 6. The first reactor REC-1 releases the highest heat of 1325.01 kW while reactor REC-7 releases the lowest amount of heat of 4.88 kW to the environment. The rejected heat from the reactors can be used for industrial services such as manufacturing ice and cooling cold stores for retail stores and cooling for medical treatment. This will increase the overall efficiency of the process since the useful energy components have been increased by using rejected heat.

The total required compressor power of both the hydrogen and

Table 6
Energy and exergy components of hydrogen liquefaction system including nitrogen and hydrogen cooling cycles.

Items	$\dot{W}$ [kW]	$\dot{Q}$ [kW]	$\dot{E}x_{des}$ [kJ/s]	η [%]	ψ [%]	Items	$\dot{Q}$ [kW]	$\dot{E}x_{des}$ [kJ/s]	η [%]	ψ [%]
CM1	22513.72	0	3397.72	80	84.91	**REC-6**	−60.96	532.27	99.57	97.73
CM2	32205.52	0	4184.32	80	87.01	**REC-7**	−4.88	1304.22	99.97	93.76
CM3	12364.58	0	1727.06	78	86.03	**REC-8**	−106.5	1918.04	99.35	92.56
CM4	13473.08	0	1732.9	78	87.14	**EX2**	0	5951.62	100	29.67
CM5	12829.6	0	1713	78	86.65	**EX3**	0	3407.04	100	71.29
ET1	−142.91	0	173.53	80	97.3	**EX4**	0	4399.95	100	8.16
ET2	−270.66	0	343.24	80	97.39	**EX5**	0	254.93	100	96.18
ET3	−6907.9	0	50419.8	90	26.18	**EX6**	0	503.3	100	96.31
NT	−4977.01	0	4795.09	80	76.17	**EX7**	0	530.5	100	99.23
CN2	0	−21922.91	1329.64	100	87.16	**EX8**	0	131	100	99.88
CN3	0	−29340.71	4915	100	86.84	**EX9**	0	19.91	100	88.36
CN4	0	−11198.07	1953.73	100	81.69	**EX10**	0	20.95	100	97.45
CN5	0	−14183.01	2854	100	85.67	**MX1-N**	0	4.32	100	99.95
CN6	0	−18497.58	1704.33	100	93.8	**MX2-N**	0	313.42	100	9.7
HX2	0	42844.52	14524.75	100	86.57	**MX1**	0	0.02	100	100
HX3	0	855.28	199.07	100	99.72	**MX2**	0	3.05	100	100
HX4	0	1304.1	2817.5	100	98.04	**MX3**	0	0.09	100	100
HX5	0	1100.86	3346.5	100	97.74	**MX4**	0	0.44	100	100
HX6	0	1039.72	85056.73	100	13.6	**MX5**	0	44.23	100	99.53
HX7	0	2184.9	15684.69	100	89.75	**MX6**	0	0.12	100	100
HX8	0	3847.79	85745.82	100	51.49	**S3–N**	0	0	100	100
HX9	0	34.54	370.95	100	99.66	**S3**	0	0	100	100
HX10	0	510.37	424.21	100	98.11	**SP1–N**	0	0	100	100
REC-1	0	−1325.01	738.66	88.54	93.99	**SP1**	0	0	100	100
REC-2	0	−84.71	257.6	99.23	98.15	**SP2**	0	0	100	100
REC-3	0	−91.2	245.95	99.22	98.49	**SP3**	0	0	100	100
REC-4	0	−353.72	1153.68	97.2	94	**SP4**	0	0	100	100
REC-5	0	−139.22	2055.26	98.96	86.4	**Total Exergy destruction [kW] 313204.2**				

Table 7
Specifications of heat exchangers in the process.

Parameter	HX2	HX3	HX4	HX5	HX6	HX7	HX8	HX9	HX10
LMTD (°C)	10.55	1.57	9.35	7.89	8.58	9.42	9.39	9.35	18.14
MTA (°C)	1.20	1.00	2.21	1.75	1.75	2.10	1.40	2.10	2.48
No. of Paths	5	2	4	4	4	4	3	2	2
Heat duty (kW)	42844.52	855.28	1304.10	1100.86	1039.72	2184.90	3847.79	34.54	510.37

Table 8
Mass fraction of conversion products of normal and para-hydrogen at reactor conditions.

Reactor	T [K]	Para-H_2, X_p	Normal H_2 (1-X_p)	Total Para-H_2 Y_p	C_0	C_1	C_2	K [%]
REC-1	70	0.413	0.587	0.556	41.22	−1.57E-02	2.24E-04	41.3
REC-2	80	0.314	0.686	0.486	31.38	−1.38E-02	1.72E-04	31.4
REC-3	68	0.413	0.587	0.560	41.28	−1.62E-02	2.38E-04	41.3
REC-4	56	0.772	0.228	0.829	77.18	−1.96E-02	3.51E-04	77.2
REC-5	44	0.905	0.095	0.929	90.48	−2.50E-02	5.68E-04	90.5
REC-6	30	0.96	0.04	0.970	95.98	−3.67E-02	1.22E-03	96.0
REC-7	22	0.99	0.01	0.993	98.97	−5.00E-02	2.27E-03	99.0
REC-8	20.5	0.998	0.002	0.999	99.77	−5.37E-02	2.62E-03	99.8

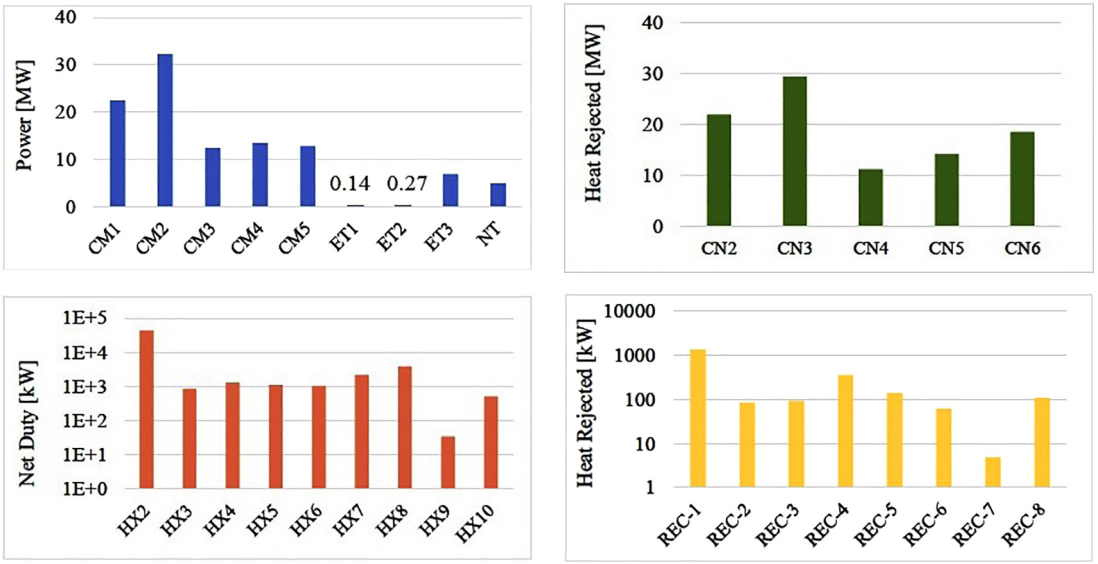

Fig. 5. Net power and heat for compressors, turbines (a), condensers (b), heat exchangers (c), and reactors (d) in the hydrogen liquefaction system.

nitrogen refrigeration cycles is estimated to be 93.4 MW, while the total turbine power of these cycles is calculated as 12.3 MW. Therefore, the total net power of hydrogen the liquefaction system is evaluated as 81.1 MW (81088.03 kW). The mass flow rate of the liquefied hydrogen is given as 3.5156 kg/s. Therefore, the specific energy consumption of the proposed system can be estimated as follows:

$$SEC = \frac{81088.03}{3.5156 \times 3600} = 6.41\ kWh \Big/ kgLH_2$$

The SEC of the current system is 6.41 kWh/kg-LH_2 to produce liquefied hydrogen of 335 t/d. which is less than that of (Matsuda and Nagami, 1997) (8.53 kWh/kg-LH_2 for 300 t/d) (Quack, 2002), (6.93 kWh/kg-LH_2 for 170 t/d), and (Baker and Shaner, 1978) (9.1 kWh/kg-LH_2 for 250 t/d).

Fig. 5 demonstrates the amount of power and heat for each component in the liquefaction system. The most power consumer is the compressor, CM2. The total power consumption of nitrogen compressors are less than that of hydrogen compressors although higher pressure ratio and mass flow rate of nitrogen cycle. Similarly, the rejected heat from condensers of hydrogen refrigeration cycle is higher than that of the nitrogen precooling cycle. The first heat exchanger HX2 has the highest heat duty of 43 MW which is greater than the summation of all the heat duty of the remainder of heat exchangers. In addition, the first reactor releases the most heat to convert all the amount of gaseous hydrogen to about 41.3% para-hydrogen and 58.7% gaseous hydrogen at 70 K, as presented in Table 8.

Fig. 6 displays the temperature at the inlet and exit of heat exchangers for six paths starting from path 0, which refers to the nitrogen stream (states 97 and 86) to path 4 and 5, which refer to the liquefied hydrogen stream (states 19–39L). The first heat exchanger HX2 drops the temperature of hydrogen from 298 to 100 K causing the heat duty to increase from 0 to 43 MW, while the eight heat exchangers (HX3 to HX10) decrease the hydrogen temperature to 20 K releasing the amount heat of 12 MW (from 43 MW to 55 MW).

Fig. 7 illustrates the ratio of exergy destruction rate for each groups of components. Heat exchangers have the highest exergy destruction rate about 66%, followed by turbines of about 18%. The splitters and flash separators have 0% exergy destruction because they are only used for dividing the streams adiabatically. The compressors, condensers, expansion valves have exergy restoration rate of about 4%, while the irreversibility of reactors is 2.62%, respectively. Exergy destruction in heat exchanger is the highest among the components of hydrogen liquefaction system similar to (Asadnia and Mehrpooya, 2017; Sadaghiani and Mehrpooya, 2017) because the temperature difference between the cold and hot paths and the ortho-para hydrogen conversion. This increase is common in cryogenic and liquefaction processes due to the huge thermal difference and chemical reaction in the fluid medium. There are possible ways to reduce the exergy destruction of heat exchangers (Wilhelmsen et al., 2018), such as mixing hydrogen refrigerant with helium-neon mixture and using catalyst impeded within the plate-fin heat exchanger. This combination can reduce the exergy destruction of heat exchanger by 43%.

The water electrolyzer was designed to produce hydrogen gas at

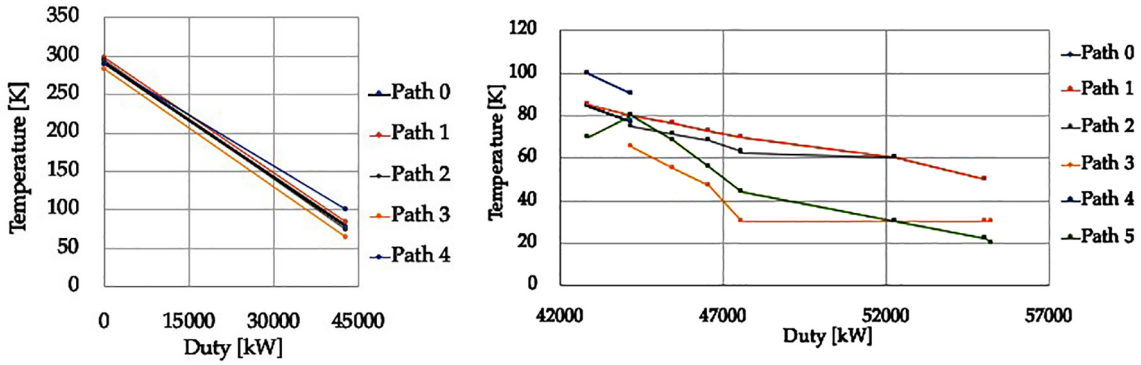

Fig. 6. Temperature and duty of heat exchangers. The left side is for HX2, while the right side is for HX3 to HX10 in the hydrogen liquefaction system.

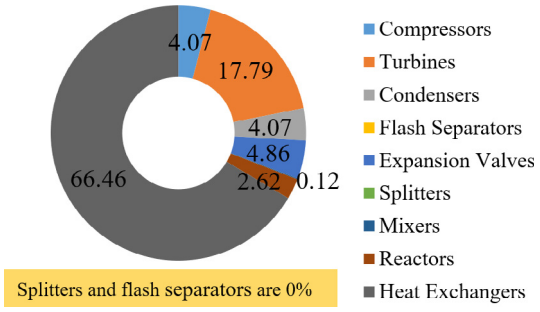

Fig. 7. Exergy destruction percentage for all components of the hydrogen liquefaction system.

a mass flow rate of 3.5156 kg/s. The amount of water was selected to 32.05 kg/s to produce 3.566 kg/s hydrogen gas. The thermodynamic properties of each state points (from 16 to 19) of the electrolyzer is tabulated in Table 9, while the required electrical power to operate the electrolyzer is about 18489 kW. The actual and theoretical COP of the electrolyzer are 21.08 and 33.34, respectively. That yields energy and exergy efficiency to be 60% and 63.3%, respectively, as shown in Table 10.

Adding the required work of the electrolyzer to the total net power of the hydrogen liquefaction, the gross net power is estimated to be 99577.1 kW (100 MW). This amount of electrical load is required to be supplied by the geothermal and isobutene cycles. The thermodynamic properties of geothermal and isobutene systems are displayed in Table 9 from state point 1 to state point 14, while the energy, exergy rates, exergy destruction, energy and exergy efficiencies are listed in Table 10.

The current power station can produce electricity at 43412 kW (43 MW). However, this is not sufficient for the hydrogen liquefaction and production of 100 MW. Therefore, it is recommended to construct three power plants of geothermal and isobutene systems. The gross net power of three stations can be evaluated as 130236 kW (130 MW) which supplies electrical load for hydrogen liquefaction and the electrical grid for community services of about 30 MW.

This integrated system has five subsystems: geothermal power plant, isobutene power plant, electrolyzer, nitrogen precooling system, and hydrogen Claude refrigeration system. The overall energy and exergy efficiency for each subsystem are listed in Table 11. The energetic and exergetic COP of the hydrogen Claude refrigeration cooling are 1.123 and 1.815 (>1), while the energetic and exergetic COP of nitrogen precooling cycle are 0.299 and 0.205 (<1). The overall energy and exergy efficiencies of the hydrogen liquefaction system are estimated as 19.78% and 63.4%, and the FOM is obtained as 0.634.

Table 9
Process stream data for geothermal and isobutene power plant and electrolyzer system.

State	$\dot{m}$ [kg/s]	T [°C]	P [kPa]	x [-]	h [kJ/kg]	s [kJ/kg.K]	ex [kJ/kg]
1	500	250	3974	0	1085	2.79	257.6
2	500	179.9	1000	0.16	1085	2.85	240.4
3	80	179.9	1000	1	2778	6.59	819.6
4	80	93.51	80	0.90	2439	6.82	412.2
5	420	179.9	1000	0	762.9	2.14	130
6	420	82.57	1000	>1	346.5	1.11	21.65
7	420	82.74	80	>1	346.5	1.11	20.86
8	80	93.51	80	0.1	619.1	1.85	71.35
9	500	93.13	80	>1	390.1	1.23	28.48
12	400	73.12	500	<1	512.5	1.65	71.99
13	400	42.71	500	0	116	0.40	47.48
14	400	43.12	1500	>1	118.2	0.40	49.27
15	400	109.7	1500	<1	555.5	1.62	121.6
16	32.09	17	200	>1	71.47	0.25	50.54
17	3.57	17	200	>1	3818	50.18	118888
18	28.52	17	200	>1	−7.902	−0.20	300.8

3.2. Parametric study results

In this section, the parametric studies were implemented on three major parts of the whole system, which includes the geothermal power plant, isobutene power plants, and the hydrogen liquefaction. They are discussed in the following subsections.

3.2.1. Parametric study on geothermal power plant

Some parametric studies have been undertaken on pressure and mass flow rate of the geothermal power plant. Fig. 8 shows the change of pressure and mass flow rate of geothermal power plant system, noting that the overall efficiency does not include the usage of the condenser rejected heat. The increase in steam mass flow rate from 300 to 700 kg/s increases the energy efficiency and the power turbine by 10% and exergy efficiency by 5% as shown in Fig. 8-a. However, increasing the inlet pressure of the turbine (P-high in Fig. 8) from 800 kPa to 2000 kPa, decreases the energy and exergy efficiency by 5% and the power turbine by 50%, as shown in Fig. 8-b, while the exit pressure from the turbine ST and mass flow rate remain constant at 80 kPa and 500 kg/s, respectively.

Fig. 8-d shows the effect of changing inlet and exit pressure of turbine ST on its power, while the steam mass flow rate remains at 500 kg/s. The highest obtained power from the turbine occurs when the inlet steam pressure increases and the exit of stream pressure from the turbine decreases. Increasing the inlet pressure from 1000 kPa to 1500 kPa has slight effect on the turbine power of

Table 10
Energy and exergy for components in the geothermal plant and isobutene power plant electrolyzer system.

Component	$\dot{W}$ [kW]	$\dot{Q}$ [kW]	$\dot{S}_{gen}$[kJ/kg.s]	$\dot{E}x_{des}$ [kJ/s]	η [%]	ψ [%]
Turbine, ST	27096	–	18.47	5505	80	91.61
Condenser, CN1	–	145631	26.87	1194	100	96.38
Separator, S1	–	–	0	0	100	100
Expansion Valve, EX1	–	–	1.12	333.5	100	96.33
Flash Chamber, FC	–	–	28.82	8625	100	93.30
Adiabatic mixing	–	–	0.77	230.8	100	98.40
Heat exchanger, HX1	–	65583	55.68	16593	100	77.67
Production Well, PW	–	**490238	*128807	–	–	–
Reinjection Well, RW	–	**142623	*14238	–	–	–
Air cooled condenser, AC	–	158572	61.11	1400	100	85.72
Isobutene turbine, IT	17198	–	8.82	2627	85	86.75
Pump, P1	882	–	0.56	166.2	80	99.16
Heat exchanger, HX1	–	65583	55.68	16593	100	77.67
Electrolyzer +	18489	–	165	412367	60	63.30

** energy rate * exergy rate + COP and COP_{th} of the electrolyzer = 21.08 and 33.34, respectively.

Table 11
Overall energy and exergy efficiencies of each subsystem and overall hydrogen liquefaction system.

Subsystem	Total Energy Input	Total Energy Output	η [%]	ψ [%]
Geothermal power plant	347615	238310	68.6	63.4
Isobutene power plant	66465	17198	25.9	69.1
Electrolyzer	18489	11093.4	60.0	63.3
Nitrogen precooling	33844.8	10118.2	29.9[a]	20.5[a]
Hydrogen refrigeration	47397.8	53211.7	112.3[a]	181.5[a]
Hydrogen Liquefaction	81088	16040.8	19.8	63.4

[a] COP in percentage.

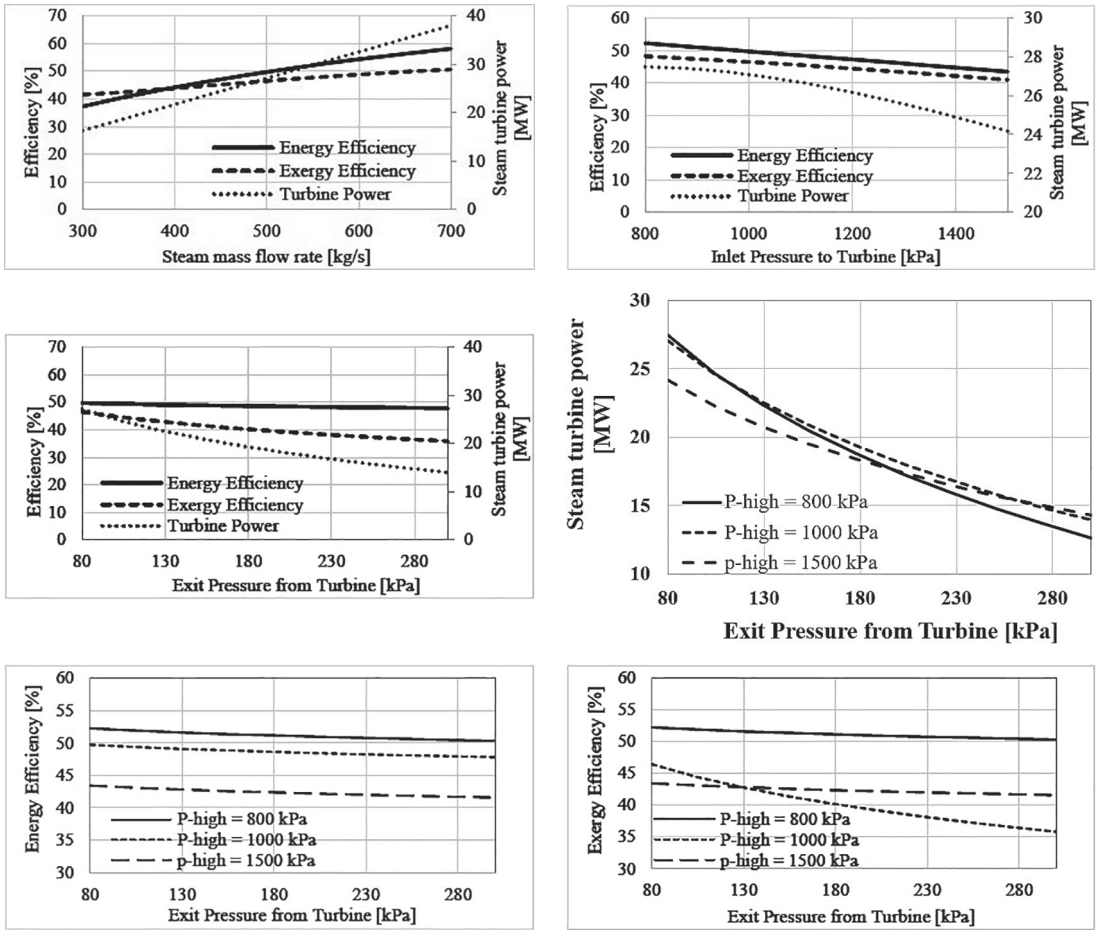

Fig. 8. Effect of steam mass flow rate, inlet pressure and exit pressure to steam turbine on energy and exergy efficiency and steam turbine power of geothermal power plant.

about 27 MW. However, the inlet pressure of both 1000 and 1500 kPa decrease the overall energy and exergy efficiency of the subsystem to less than 50%, and the efficiencies increases to be more than 50% for the inlet pressure of 800 kPa, as shown in Fig. 8-e and Fig. 8-f.

3.2.2. Parametric study on isobutene power plant

The effect of change in pressure of the turbine and pump and the isobutene mass flow rate has been studied in the isobutene power plant. Fig. 9 displays the change of pressure and mass flow rate on the isobutene power system. The increase in mass flow rate does not affect the energy and exergy efficiencies since it does not change within the cycles. However, the increase from 200 kg/s to 500 kg/s increases the net power, which is the difference between the turbine power and the pump power, by 50% (from 10 MW to 20 MW), as shown in Fig. 9-a.

Increasing the high pressure (from 1000 kPa to 2000 kPa) while decreasing the low pressure (from 800 kPa to 200 kPa) increases the net power of the isobutene power system from 15 to 35 MW, as shown in Fig. 8-b. It also increases the energy efficiency from 10% to 17%, and the exergy efficiency from 30% to 55%, as shown in Fig. 9-c and 9-d.

The highest net power from both systems are selected based on the parametric studies. For the geothermal power plant, the mass flow rate and the inlet and exit pressure of steam turbine ST can be re-evaluated to be 700 kg/s, 1000 kPa, and 80 kPa, respectively. This power cycle will produce 40 MW. For the isobutene power system, the mass flow rate, and the high and low pressure of the cycle can be re-estimated to be 500 kg/s, 2000 kPa, and 200 kPa, respectively. Thus, the net power of the isobutene cycle will be determined as 35 MW. Therefore, the total power delivered from both subsystems multiplied by three stations is determined to be 225 MW.

3.2.3. Parametric study on HCR

The parametric studies were also implemented on the hydrogen Claude refrigeration system in terms of changing the high pressure and mass flow rate using Aspen Plus software since this system consumes more power than the nitrogen precooling cycle. Three levels of the high pressure are selected 2000 kPa, 3000 kPa, and 5000 kPa, and two levels of mass flow rate are chosen 14 kg/s and 9 kg/s. Fig. 9 displays the changes in mass flow rates and in the high pressure compressor. The intermediate pressure of MPP is a function of the high pressure and low pressure following this relationship: $P_{mid} = \sqrt{P_{high} \times P_{low}}$, where the lower pressure is constant at 200 kPa.

The mass flow rate for hydrogen refrigeration cycle is 14 kg/s, increasing the high pressure from 2000 kPa to 5000 kPa increases the condenser rejected heat by about 20%. While this increase does not affect the duty of heat exchangers (Fig. 9-a), however, decreasing the mass flow rate by 35% to 9 kg/s, decreases the rejected heat from the condensers by 20% for high pressure of 5000 kPa and 35% for the 2000 kPa. It also decreased the duty of heat exchangers by 35% with respect to the primary case of mass flowrate of 14 kg/s (i.e., inside the red box of Fig. 9-b).

In addition, the net power increased to 105 MW at the high pressure of 5000 kPa, while it reached 78 MW at 2000 kPa for a hydrogen mass flow rate of 14 kg/s, as shown in Fig. 10-c. Moreover, the net power decreased by about 35% from 78 MW to 60 MW at the high pressure of 2000 kPa and by 18% for 5000 kPa for a mass flow rate of 9 kg/s, as shown in Fig. 10-d.

This change in the high pressure and mass flow rate of hydrogen refrigeration cycle have a significant impact on the specific energy consumption of the overall hydrogen liquefaction system, as shown in Fig. 11. The minimum SEC that can be achieved at 4.7 kWh/kg-LH_2 for mass flow rate of 9 kg/s and minimum high pressure of 2000 kPa. This will increase the exergy efficiency of the hydrogen liquefaction to 85.7%.

3.2.4. Comparison of hydrogen liquefaction process

In order to validate the presented design, comparison among other studies of hydrogen liquefaction is considered to evaluate the proposed system for the large scale, as shown in Table 12. This comparsion was focused on the net power of the whole process including precooling and cryogenic cycles, and the liquefied stream, the enthalpy and the exergy flow rate of feed and product of liquefied hydrogen, the energy efficiency and exergy efficiency based on equations (16) and (17), and the SEC and SEC min according to eqautions (18) and (19).

Note that the proposed study have achieved lower SEC than that of (Asadnia and Mehrpooya, 2017), (Ansarinasab et al., 2017), (Baker and Shaner, 1978) by 20%, 46.6%, and 69.4%, respectively. However, the current research have obtianed more SEC than that of (Berstad

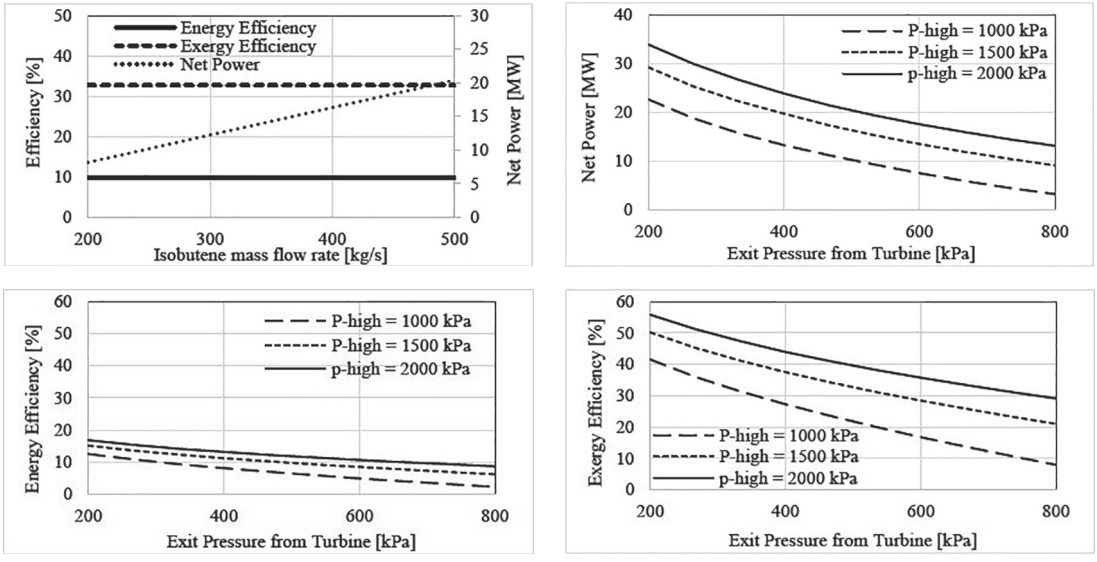

Fig. 9. Effect of isobutene mass flow rate, high pressure and low pressure on energy and exergy efficiency and turbine power of isobutene power plant.

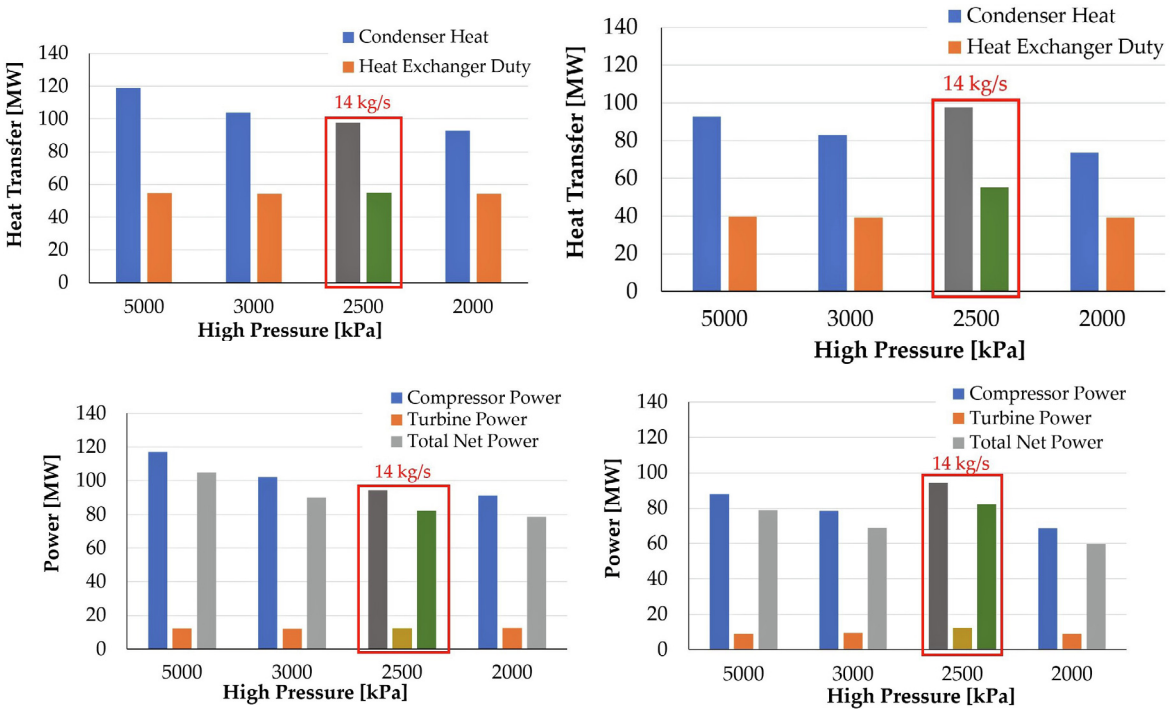

Fig. 10. The effect of change in mass flow rate and high compressor pressures on heat duty and net power of the hydrogen liquefaction system.

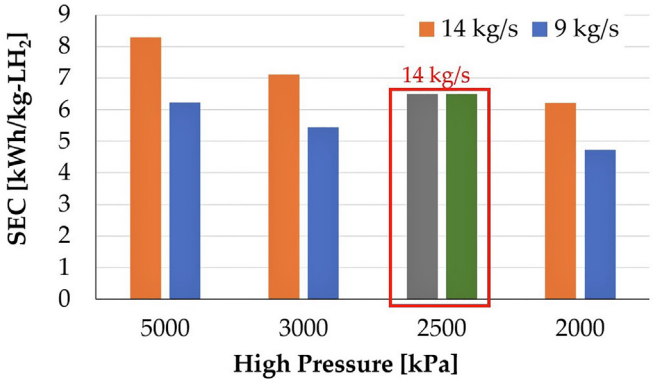

Fig. 11. The effect of high pressure and mass flow rate on SEC of the liquefaction system.

et al., 2010), Ansarinasab et al. (2019), and (Valenti and Macchi, 2008) by 1.1%, 33.5%, and 21.4%, respectively. The current liquefaction process has been optimized, so the SEC is obtianed to be 4.74 kWh/kg-LH_2, which is lower than that of most studies except (Ansarinasab et al., 2019) of 4.26 kWh/kg-LH_2. The exergy efficiency of different liquefaction processes have a range of 13.20–47.73, while the current process have achieved an exergy efficiency of 63.4% and can be increased to 85.7%. For the energy efficiency, most studies have a range of 10.30%–20.34%. The proposed research has fulfilled the energy efficiency to be 19.8%, while the energy efficiency of the optimized one reaches to 26.74%.

4. Conclusions

This paper presents a novel approach of a comprehensively integrated large-scale hydrogen liquefaction system combined with a water electrolyzer, a geothermal power plant and an isobutene power plant. The selected power plants are employed as subsystems to provide clean and sustainable electric power using non-fossil fuel alternatives.

- Two refrigeration cycles are used to liquefy the hydrogen produced: hydrogen Claude refrigeration system and nitrogen precooling system to produce 335 ton/day of liquefied hydrogen. The mass flow rates of hydrogen in the hydrogen Claude refrigeration and nitrogen precooling systems are 14 kg/s and 52 kg/s, respectively. The overall power consumption of the liquefaction process is determined to be 81.1 MW with a specific energy consumption of 6.41 kWh/kg-LH_2. The energy and exergy efficiencies of the process are found to be 19.8% and 63.4%, respectively.
- A water electrolyzer is used to split the water electrochemically at a mass flow rate of 32.05 kg/s of fresh water to obtain 3.566 kg/s of gaseous hydrogen. The required power for the electrolyzer is estimated to be 18.5 MW. Therefore, the total power consumption of the hydrogen liquefaction and the electrolyzer is about 100 MW, which requires constructing three power plants running with a geothermal energy and the isobutene power cycles. The gross electrical load from the three power plants is 130 MW, which appears to be sufficient for the liquefaction system and for powering community services.
- Some parametric studies have been carried out in order to improve the system performance. The net electric power of three stations is increased by 73%–225 MW. This increase is achieved by increasing the pressure ratio of the turbines to 12.5 and 10, and increasing the mass flow rate by 40% and 100% for the geothermal and isobutene power plants, respectively. The performance of the liquefaction process is further improvided by implementing an HCR to reduce the power consumption and increase the energy and exergy efficiencies. As a result, the high pressure of the hydrogen refrigeration cycle was decreased by 25%-, and hydrogen mass flow rate by 56% -. This yields a reduction in the net power consumption of 60 MW and SEC to 4.7 kWh/kg-LH_2 instead of 81 MW and 6.41 kWh/kg-LH_2.

Table 12
Comparison of previous studies regarding the net power and energy and exergy efficiencies and SEC.

Reference	$\dot{m}_{LH_2}$ [kg/s]	$\dot{W}_{net}$ [kW]	h_{feed} [kJ/kg]	$h_{product}$ [kJ/kg]	$\eta_{overall}$ [%]	$\dot{E}x_{feed}$ [kW]	$\dot{E}x_{product}$ [kW]	$\psi_{overall}$ [%]	SEC kWh/kg-LH_2
(Asadnia and Mehrpooya, 2017)	1.157 Feed: 298K & 21 bar Products: 20.2K & 1.3 bar	32030	−0.7	−4733	17.1	4323	16984	39.5	7.69 $SEC_{min} = 3.04$
(Berstad et al., 2010)	1 Feed: 310K & 21 bar Product: 20.2K & 1 bar	22808 23343 22146	–	–	–	–	–	45.77 44.73 47.14	6.34 6.48 6.15 $SEC_{min} = 3.04$
(Ansarinasab et al., 2017)	1.157 Feed: 298K & 21 bar Product: 20.2K & 1.3 bar	39194.15	−0.7	−4357.27	12.86	14120	148312	18.16	9.40 $SEC_{min} = 1.71$
(Ansarinasab et al., 2019) [a]	3.45 Feed: 298K & 21 bar Product: 20.2K & 1.3 bar	52851	−1	−2786	18.18	414045	421020	13.20	4.26 $SEC_{min} = 0.56$
(Sadaghiani et al., 2017)	1.5 Feed: 298K & 21 bar Product: 20.2K & 1.3 bar	40590.11	−1	−2788.14	10.30	171724	180912	22.64	7.52 $SEC_{min} = 1.70$
(Aasadnia and Mehrpooya (2018))	1.033 Feed: 298K & 21 bar Product: 20.2K & 1.3 bar	24052.38	−0.7	−4736	20.34	4323	15183	45.15	6.47 $SEC_{min} = 2.92$
(Baker and Shaner, 1978)	2.90 Feed: 308K & 1.01 bar Product: 20.57K & 9.29 bar	113110.5 $\dot{W}_{min} = 40711.8$	–	–	–	–	–	36.0	10.86 $SEC_{min} = 3.91$
(Valenti and Macchi, 2008)	10 Feed: 300K & 60 bar Product: 20.0K & 1.5 bar	181400 $\dot{W}_{net} = 86590$	–	–	–	–	–	47.73	5.04 $SEC_{min} = 2.41$
Purposed research	3.5156 Feed: 290K & 2 bar Product: 20.2K & 1.3 bar	81088 60154 [b]	−115.74	−4678.62	19.8 26.74 [b]	838.376	15467.1	63.4 85.71 [b]	6.41 4.74 [b] $SEC_{min} = 4.06$

[a] Ansarinasab et al. (2019) have recorded SEC and exergy efficiency for the last liquefaction stage as 1.102 kWh/kg-LH_2 and 55.47%, but the SEC and $\psi_{overall}$ in this table have been calculated for overall process.
[b] Optimized liquefaction process by changing the mass flow rate and pressure path of hydrogen Claude refrigeration cycle.

Therefore, both energy and exergy efficiencies of the entire process are improved by 26.74% and 63.4–85.71%, respectively.

In closing, the unique design of the present system offers a cleaner production of hydrogen through an integrated liquefaction system powered by geothermal energy. This is considered an eco-freindly approach for power production in order to improve the environmental sustainability.

It is planned to have future studies focusing on comprehensive cost assessment and multiobjective optimization of the present system. In addition, the renewable energy sources such as solar, wind, biomass and ocean could be enhanced. Furthermore, exergoeconomic and exergoenvironmental studies are to ne undertaken for better analysis and assessment of the proposed system for practical applications.

Acknowledgement

This research is supported by the The Natural Sciences and Engineering Research Council of Canada (NSERC).

References

Aasadnia, M., Mehrpooya, M., 2018. Conceptual design and analysis of a novel process for hydrogen liquefaction assisted by absorption precooling system. J. Clean. Prod. 205, 565–588. https://doi.org/10.1016/j.jclepro.2018.09.001.
Ansarinasab, H., Mehrpooya, M., Mohammadi, A., 2017. Advanced exergy and exergoeconomic analyses of a hydrogen liquefaction plant equipped with mixed refrigerant system. J. Clean. Prod. 144, 248–259. https://doi.org/10.1016/j.jclepro.2017.01.014.
Ansarinasab, H., Mehrpooya, M., Sadeghzadeh, M., 2019. An exergy-based investigation on hydrogen liquefaction plant-exergy, exergoeconomic, and exergoenvironmental analyses. J. Clean. Prod. 210, 530–541. https://doi.org/10.1016/j.jclepro.2018.11.090.
Asadnia, M., Mehrpooya, M., 2017. A novel hydrogen liquefaction process configuration with combined mixed refrigerant systems. Int. J. Hydrogen Energy 42, 15564–15585. https://doi.org/10.1016/j.ijhydene.2017.04.260.
Baker, C.R., Shaner, R.L., 1978. A study of the efficiency of hydrogen liquefaction. Int. J. Hydrogen Energy 3, 321–334. https://doi.org/10.1016/0360-3199(78)90037-X.
Berstad, D.O., Stang, J.H., Neksa, P., 2010. Large-scale hydrogen liquefier utilising mixed-refrigerant. Int. J. Hydrogen Energy 35, 4512–4523. https://doi.org/10.1016/j.ijhydene.2010.02.001.
Bracha, M., Lorenz, G., Patzelt, A., Wanner, M., 1994. Large-scale hydrogen liquefaction in Germany. Int. J. Hydrogen Energy 19, 53–59. https://doi.org/10.1016/0360-3199(94)90177-5.
Cardella, U., Decker, L., Sundberg, J., Klein, H., 2017. Process optimization for large-scale hydrogen liquefaction. Int. J. Hydrogen Energy 42, 12339–12354. https://doi.org/10.1016/j.ijhydene.2017.03.167.
Carmo, M., Fritz, D.L., Mergel, J., Stolten, D., 2013. A comprehensive review on PEM water electrolysis. Int. J. Hydrogen Energy 38, 4901–4934. https://doi.org/10.1016/j.ijhydene.2013.01.151.
Dincer, I., Acar, C., 2014. Review and evaluation of hydrogen production methods for better sustainability. Int. J. Hydrogen Energy 40, 11094–11111. https://doi.org/10.1016/j.ijhydene.2014.12.035.
Dincer, I., Zamfirescu, C., 2016. Sustainable Hydrogen Production. Elsevier Inc. Joe Hayton. https://doi.org/10.1126/science.1103197.
Krasae-in, S., Stang, J.H., Neksa, P., 2010. Development of large-scale hydrogen liquefaction processes from 1898 to 2009. Int. J. Hydrogen Energy 35, 4524–4533. https://doi.org/10.1016/j.ijhydene.2010.02.109.
Leachman, J.W., Jacobsen, R.T., Penoncello, S.G., Lemmon, E.W., 2009. Fundamental equations of state for parahydrogen, normal hydrogen, and orthohydrogen. J. Phys. Chem. Ref. Data 38, 721–748. https://doi.org/10.1063/1.3160306.
Matsuda, H., Nagami, M., 1997. Study of large hydrogen liquefaction in process. Hydrog. Energy 8, 175–175.
McCarty, R.D., Hord, J., Roder, H.M., 1981. Selected Properties of Hydrogen.
Mohammadi, A., Mehrpooya, M., 2018. A comprehensive review on coupling different types of electrolyzer to renewable energy sources. Energy 158, 632–655. https://doi.org/10.1016/j.energy.2018.06.073.
Noh, J., Fulgueras, A.M., Sebastian, L.J., Lee, H.G., Kim, D.S., Cho, J., 2017. Estimation of thermodynamic properties of hydrogen isotopes and modeling of hydrogen isotope systems using Aspen Plus simulator. J. Ind. Eng. Chem. 46, 1–8. https://doi.org/10.1016/j.jiec.2016.07.053.
Ohlig, K., Decker, L., 2014. The latest developments and outlook for hydrogen liquefaction technology. AIP Conf. Proc. 1573, 1311–1317. https://doi.org/10.1063/1.4860858.
Peng, D.Y., Robinson, D.B., 1976. A new two-constant equation of state. Ind. Eng.

Chem. Fundam. 15, 59–64. https://doi.org/10.1021/i160057a011.
Quack, H., 2002. Conceptual design of a high efficiency large capacity hydrogen liquefier. In: In AIP Conference Proceedings, pp. 255–263. AIP Conference Proceedings. https://doi.org/10.1063/1.1472029.
Ratlamwala, T.A.H., Dincer, I., Gadalla, M.A., Kanoglu, M., 2012. Thermodynamic analysis of a new renewable energy based hybrid system for hydrogen liquefaction. Int. J. Hydrogen Energy 37, 18108–18117. https://doi.org/10.1016/j.ijhydene.2012.09.036.
Sadaghiani, M.S., Mehrpooya, M., 2017. Introducing and energy analysis of a novel cryogenic hydrogen liquefaction process configuration. Int. J. Hydrogen Energy 42, 6033–6050. https://doi.org/10.1016/j.ijhydene.2017.01.136.
Sadaghiani, M.S., Mehrpooya, M., Ansarinasab, H., 2017. Process development and exergy cost sensitivity analysis of a novel hydrogen liquefaction process. Int. J. Hydrogen Energy 42, 29797–29819. https://doi.org/10.1016/j.ijhydene.2017.10.124.
Uyar, T.S., Beşikci, D., 2017. Integration of hydrogen energy systems into renewable energy systems for better design of 100% renewable energy communities. Int. J. Hydrogen Energy 42, 2453–2456. https://doi.org/10.1016/j.ijhydene.2016.09.086.
Valenti, G., Macchi, E., 2008. Proposal of an innovative, high-efficiency, large-scale hydrogen liquefier. Int. J. Hydrogen Energy 33, 3116–3121. https://doi.org/10.1016/j.ijhydene.2008.03.044.
Wagner, S., 2014. Conversion rate of para-hydrogen to ortho-hydrogen by oxygen: implications for PHIP gas storage and utilization. Magn. Reson. Mater. Phys., Biol. Med. 27, 195–199. https://doi.org/10.1007/s10334-013-0399-y.
Wilhelmsen, Ø., Berstad, D., Aasen, A., Nekså, P., Skaugen, G., 2018. Reducing the exergy destruction in the cryogenic heat exchangers of hydrogen liquefaction processes. Int. J. Hydrogen Energy 43, 5033–5047. https://doi.org/10.1016/j.ijhydene.2018.01.094.
Won, W., Kwon, H., Han, J.H., Kim, J., 2017. Design and operation of renewable energy sources based hydrogen supply system: technology integration and optimization. Renew. Energy 103, 226–238. https://doi.org/10.1016/j.renene.2016.11.038.